Energy Conversion and Management 66 (2013) 1–10

Contents lists available at SciVerse ScienceDirect

Energy Conversion and Management

journal homepage: www.elsevier.com/locate/enconman

Optimization of energy extraction for vertical closed-loop geothermal systems considering groundwater flow

Jozsef Hecht-Méndez [a,*], Michael de Paly [b], Markus Beck [b], Peter Bayer [c]

[a] University of Tübingen, Center for Applied Geoscience (ZAG), Sigwartstrasse 10, 72076 Tübingen, Germany
[b] University of Tübingen, Wilhelm-Schickard-Institute for Computer Science (WSI), Sand 1, 72076 Tübingen, Germany
[c] ETH Zurich, Engineering Geology, Sonneggstrasse 5, 8092 Zürich, Switzerland

ARTICLE INFO

Article history:
Received 28 December 2011
Received in revised form 12 September 2012
Accepted 14 September 2012

Keywords:
Borehole heat exchanger
BHE field
Groundwater flow
Optimization
Moving line source
FEFLOW

ABSTRACT

A combined simulation–optimization procedure is presented to regulate the operation of borehole heat exchangers (BHEs) in a multiple BHE field when groundwater flow exists. Such fields are of increasing interest for large-scale geothermal heating energy supply of buildings, but so far strategic adjustment of energy extraction rates (loads) of the individual BHEs has not been considered in practice. Groundwater flow means an additional advective energy supply, which is advantageous but also complicates proper BHE adjustment. In the presented procedure, the field is simulated by temporally and spatially superimposed moving line source equations. The optimization goal is formulated in an objective function to minimize the thermal impact in the ground, to avoid extreme temperature anomalies, and by this, ultimately improve heat pump performance. For a given seasonal energy demand and total operation time, linear programming efficiently delivers optimized BHE operation patterns. For an examined square lattice of 25 BHEs, the optimized radial load patterns characteristic for conduction dominated conditions change to patterns that are oriented at the groundwater flow when advection dominates. Through this, optimization always levels the temperature distribution in the ground. Also, in comparison to routine practice, mean BHE outlet temperatures can be increased. For the small study case, numerical simulation reveals that already more than 1 K can be achieved, given a seasonal energy demand oriented at common conditions in central Europe. However, for a fixed energy demand, advective heat supply towards the BHEs increases with groundwater flow velocity and thus mitigates the benefits from optimization.

1. Introduction

Vertical ground source heat pumps (GSHPs) are routine devices of shallow geothermal energy use. In the most common case, they are employed for space heating of buildings. Alternatively GSHPs may also serve cooling purposes. The prevalent variants, such as in the dominating markets of Europe, are mini-systems that supply individual residential houses with an installed power ranging between 10 kW and 12 kW [1–3]. One, or a small number of adjacent boreholes are drilled down to a depth of typically 50–150 m, and by continuous circulation of a carrier fluid, heat is collected from the ambient underground. The heat is transported to a heat pump in the building to feed the space and/or hot water heating unit, and then the heat carrier fluid is returned to the ground loop. This ground loop most often represents a piped circuit system installed within the borehole, the borehole heat exchanger (BHE), which is separated from the ground and extracts heat solely by conduction.

Meanwhile, large-scale applications to supply hotels, greenhouses, schools, big office buildings or district heating systems are growing in number [4–6]. A higher energy demand is supplied by extraction of heat from larger volumes of the subsurface. This is achieved by running galleries of multiple BHEs. In contrast to the design of single BHE systems, such multiple neighboring BHEs can interact and influence each other. This could have an effect on the overall system's performance and hence, should be either avoided or integrated in the operation strategy [7,8]. Proficient operation of BHE fields often also has to account for the effects of seasonal use. This means that the ground chilled in the cold seasons needs intermittent summer periods to slowly recover and at least partly "recharge the battery". In fact, the lower the temperature in the ground, the less efficient the GSHP is. In order to guarantee sustainable use, i.e. at lower than maximum possible production level but with satisfactory performance [9], the intensity of local temperature anomalies in the BHE field needs to be minimized while recharge during the recovery period is maximized.

Identifying an optimal BHE field design for given subsurface conditions and specific annual energy requirements is challenging,

* Corresponding author. Tel.: +49 7071 2973172; fax: +49 7071 295059.
E-mail address: jozsef.hecht-mendez@uni-tuebingen.de (J. Hecht-Méndez).

0196-8904/$ - see front matter © 2012 Elsevier Ltd. All rights reserved.
http://dx.doi.org/10.1016/j.enconman.2012.09.019

Nomenclature

C	volumetric heat capacity (J m^{-3} K^{-1})
c	specific heat capacity (J kg^{-1} K^{-1})
d	borehole diameter (m)
E_r	total energy demand for each time step (W)
K	hydraulic conductivity (m s^{-1})
k	running index of BHEs (–)
L	length of the BHE (m)
L'	characteristic length (m)
m	number of time steps (–)
n	porosity (–)
Pe	Péclet number (–)
p	number of BHEs (–)
Q	volumetric flow rate (m^3 s^{-1})
q	power demand/load (W)
q'	heat extraction rate per unit length (W m^{-1})
R_a	internal thermal resistance of the borehole (mK W^{-1})
R_b	thermal resistance of the borehole (mK W^{-1})
r	running index of the time steps (–)
T	temperature (K)
T_u	undisturbed temperature (°C)
$\Delta\overline{T}$	mean temperature change (K)
T_{out}	temperature at the BHE outlet (°C)
$\overline{T}_{out}$	mean mixed outlet temperature for all BHEs (°C)
t	time (s)
u	specific discharge (Darcy velocity) (m s^{-1})
v_a	seepage velocity (m s^{-1})
w	weighting factor (–)
x_k	coordinate of BHE k in x-direction (m)
y_k	coordinate of BHE k in y-direction (m)
z	coordinate in z-direction (m)
ρ	density (kg m^{-3})
μ	dynamic fluid viscosity (kg m^{-1} s^{-1})
λ	thermal conductivity (W m^{-1} K^{-1})
α	dispersivity (m)
ϕ	integration variable (–)
ω	response factor (–)

Subscripts

s	solid
w	water
m	porous media (solid and water)
l	longitudinal
t	transversal

considering the degrees of freedom in design and operation mode. Available design software such as EED, GLHEPRO or TRNSYS-DST [10–12], provide solutions with simplifying assumptions. For example, the underlying concepts ignore the potential of individually adjusting BHE operation. In de Paly et al. [13], we demonstrate for a hypothetical case that temporally and spatially variable energy extraction of BHEs can improve the overall system's performance and mitigate long-term temperature decline. Temperature changes in the underground are simulated by superimposed line source equations that only consider conductive heat transport. For a given configuration, the optimal operation mode is searched for by linear programming. The present study builds up on this work, and extends it to those conditions where groundwater flow in the subsurface cannot be neglected. The particular questions are: How does groundwater flow influence optimal BHE field design, and can the efficiency be improved if the effect of advective heat transport by moving groundwater is pro-actively included in the developed operation strategy? A real-case oriented setup is used to derive general conclusions on optimal individual BHE operation depending on the location of BHEs and hydrogeological conditions. In the following, related works are shortly reviewed, which particularly discuss the role of groundwater flow for shallow geothermal systems. Note that instead of the term "advection" often "convection" is used. Here, we prefer advection, as it exclusively relates to heat transport by moving groundwater, whereas convection includes all effects from fluid motion including density-driven transport.

In one of the first studies on the influence of heat advection for BHEs, Eskilson [14] concluded that the effect of groundwater flow is negligible. For a simple example, the borehole wall temperature is estimated using a groundwater flow velocity (specific discharge) of 1.5×10^{-8} m s^{-1}, showing a change of 2% in comparison to a pure conductive scenario (no flow). The used flow velocity is considered a representative average value for rocks. However, flow velocities in porous media can vary among several orders of magnitude. Recently, others have shown that the presence of groundwater flow indeed can be relevant for the heat transport around BHEs. Sutton et al. [15], Diao et al. [7] and Molina-Giraldo et al. [16,17] developed a transient analytical solution based on the moving line source theory [18] that accounts for conductive and advective heat transport. A common conclusion is that temperature distribution obtained by simulating conduction only produces errors that substantially rise with increasing groundwater flow velocity.

The modelling studies by Chiasson et al. [19] and Haehnlein et al. [20] show that when groundwater flow is present, the temperature changes in the underground surrounding the BHE are invariant after shorter operation time (i.e. steady state is reached faster). Chiasson et al. [19] also compare the performance of a BHE field adjusted by advection-free BHE design software to that simulated by the numerical model with groundwater flow. Their results indicate large differences among the predicted ground temperatures. Fan et al. [21] evaluate the performance of multiple BHEs connected to a hybrid GSHP system, using a finite volume simulation method. They find that the influences of the groundwater on the heat transfer between the BHE and the surrounding soil depends on the system operation mode and the flow velocity. The numerical modelling study by Lee and Lam [22] is dedicated to the influence of groundwater flow direction on BHE fields. They conclude that square BHE configurations are likely to be less affected than non-square setups. Wang et al. [23] quantifies the heat transfer enhancement due to the presence of groundwater flow in an in situ BHE field experiment. Average fluid temperatures within the BHE were measured for two heat extraction and two heat injection operation conditions. Comparisons with numerical results of a conductive scenario show a heat transfer rate improvement by 12.9% and 9.8% for energy extraction and injection, respectively.

In contrast to these previous, mostly process-based studies, our purpose is on integrating the potentially beneficial effects of natural groundwater flow, in order to optimize the performance of GSHP systems. Only one study, by Fujii et al. [4], is found that similarly focuses on optimization of GSHP systems, including groundwater flow. In their work, four different heat extraction and storage schemes are examined to optimize the performance of a field of 75 BHEs installed in Akita, Japan. Ground temperatures are simulated for a period of 50 years. Although the prevalent groundwater flow

velocity is insufficient to remarkably enhance the heat transfer to the geothermal system, it influences the temperature distribution and the heat extraction rate of the BHEs. Depending on operation scheme and BHE spacing, BHEs located upstream of the flow direction show higher energy extraction rates than those at downstream locations.

As shown, for instance, in Fujii et al. [4] and de Paly et al. [13], ground temperature changes in BHE fields are spatially variable, and may become significant in the long term. Control and minimization of the overall underground temperature change is in favor of the entire GSHP system performance (e.g., [24]). At the same time, regulations often constrict the maximum allowed temperature changes, in order to keep the induced temperature variations within a range that is not of environmental concern [25,26]. Groundwater flow adds complexity to simulation and control of the ground thermal regime. The heat supplied by advection is an attractive additional source, which, if used strategically, may enhance the overall system's efficiency and regeneration. In the present work, the optimization procedure developed by de Paly et al. [13] is extended for considering the effects of the groundwater flow. The approach consists of three steps: (i) fast analytical simulation of heat transport in the ground; (ii) application of iterative optimization procedure with analytical calculations; and (iii) detailed inspection of the optimized solutions with more precise numerical model.

A two-dimensional transient analytical approach, which describes conductive and advective heat transport in porous media, is included in a simulation–optimization procedure. Based on the superposition principle, temperature changes in the underground due to multiple BHEs are evaluated using monthly variable energy loads. As an objective we define the minimization of the maximal underground temperature change for given total operation time. Concurrently, the BHE field has to fulfill a given annual and monthly variable heating energy demand. Equivalent to de Paly et al. [13], the optimization procedure is applied to a case with 25 BHEs. For this case, optimized solutions are investigated for a range of different groundwater flow velocities.

2. Mathematical background

2.1. Heat transport in porous media

The governing equation for transient heat conductive and advective transport in porous media, based on the principle of heat conservation, is [27]:

$$\left(\frac{\rho_m c_m}{n\rho_w c_w}\right)\frac{\partial T}{\partial t} - div\left[\left(\frac{\lambda_m}{n\rho_w c_w} + \alpha v_a\right) grad T\right] + div(v_a T) \pm \frac{q}{n\rho_w c_w} = 0 \quad (1)$$

The first term is the storage term, and the second term describes heat conduction and dispersion, with an added advective component that represents heat transported at seepage velocity, v_a. The last term accounts for the energy source given as a heat flux or thermal load, q. In Eq. (1), thermal equilibrium between the solid and fluid phases is presumed.

Assuming an infinite homogeneous porous media at a constant uniform initial temperature, T_u, Metzger et al. [28] introduced a two-dimensional transient analytical solution for Eq. (1), based on the line source model. By this, the transversal temperature distribution, due to an infinite line source aligned with the z-axis can be estimated. At the source a constant heat flux per unit length q is assigned. Molina-Giraldo et al. [16] applied this equation to simulate the thermal anomaly from single BHE operation. The temperature difference ($\Delta T = T - T_u$) for a time t is:

$$\Delta T(\Delta x, \Delta y, t) = \frac{q}{4\pi L\sqrt{\lambda_l \lambda_t}} \exp\left(\frac{\rho_w c_w n v_a \Delta x}{2\lambda_l}\right) \times \int_0^{\frac{(\rho_w c_w n v_a)^2 t}{4\rho_m c_m \lambda_l}} \exp\left[-\left(\frac{\Delta x^2}{\lambda_l} + \frac{\Delta y^2}{\lambda_t}\right) \times \frac{(\rho_w c_w n v_a)^2}{16\lambda_l \phi} - \phi\right] \frac{d\phi}{\phi} \quad (2)$$

where $\Delta x = (i - x_k)$ and $\Delta y = (j - y_k)$ are the distances to an arbitrary location (i, j) with respect to a BHE centered at (x_k, y_k). Further parameters are

$$\lambda_l = \lambda_m + \alpha_l \rho_w c_w n v_a \quad (3)$$

$$\lambda_t = \lambda_m + \alpha_t \rho_w c_w n v_a \quad (4)$$

as the effective thermal conductivity in the longitudinal (Eq. (3)) and transverse direction (Eq. (4)), respectively [16,29]. Since Eq. (2) is linear, and assuming that the ground thermal properties do not depend on temperature, this equation can be spatially and temporally superimposed, similar to the approach in [13] for the infinite line source analytical solution without groundwater flow. This allows flexible simulation of multiple BHE fields at temporally variable loads:s

$$\Delta T_{i,j}(t, q_{1\ldots p,1\ldots m}) = \sum_{r=1}^{m}\sum_{k=1}^{p} q_{k,r}\left(\frac{1}{4\pi L\sqrt{\lambda_l \lambda_t}} \exp\left(\frac{\rho_w c_w n v_a \Delta_x}{2\lambda_l}\right) \times \left(\int_0^{\frac{(\rho_w c_w n v_a)^2 (t - t_{r-1})}{4\rho_m c_m \lambda_l}} \exp\left[-\left(\frac{\Delta x^2}{\lambda_l} + \frac{\Delta y^2}{\lambda_t}\right) \times \frac{(\rho_w c_w n v_a)^2}{16\lambda_l \phi} - \phi\right] \frac{d\phi}{\phi} - \int_0^{\frac{(\rho_w c_w n v_a)^2 (t - t_r)}{4\rho_m c_m \lambda_l}} \exp\left[-\left(\frac{\Delta x^2}{\lambda_l} + \frac{\Delta y^2}{\lambda_t}\right) \times \frac{(\rho_w c_w n v_a)^2}{16\lambda_l \phi} - \phi\right] \frac{d\phi}{\phi}\right)\right) = \sum_{r=1}^{m}\sum_{k=1}^{p} q_{k,r}\omega_{k,r}^{t,i,j} \quad (5)$$

where p is the number of BHEs and m is the number of time steps. The temperature difference at a location (i, j) is obtained by the sum of the temperature differences exerted by each individual BHE k, with load q'_r (with $q'_r = q_r/L$) applied during time step r. Using Eq. (5), the ground temperature change from multiple BHEs, each with different time variable energy loads, including advective heat transport, can be estimated.

The term $\omega_{k,r}^{t,i,j}$ represents the response factor of BHE k at a position (i, j) within the BHE field at time step $r \in \{1, \ldots, m\}$, with reference to the current time step $t \in \{1, \ldots, m\}$ and $r \leqslant t$, given $\Delta x = (i - x_k)$ and $\Delta y = (j - y_k)$. By merging $q'_{k,r}$ and $\omega_{k,r}^{t,i,j}$ into vectors of the form $\vec{q} = (q'_{1,1}, \ldots, q'_{p,1}, \ldots, q'_{p,m})$ and $\vec{\omega}^{t,i,j} = \left(\omega_{1,1}^{t,i,j}, \ldots, \omega_{p,1}^{t,i,j}, \ldots, \omega_{p,m}^{t,i,j}\right)$, Eq. (5) is rewritten as:

$$\Delta\vec{T}_{i,j}(t, \vec{q}) = \vec{q}(\vec{\omega}^{t,i,j})^T \quad (6)$$

where $\Delta\vec{T}_{i,j}(t, \vec{q})$ is the actual temperature change in the underground at position (i, j) and time step t, derived from the superposition of all BHEs in the field with the temporal load pattern $\vec{q}$.

2.2. Linear optimization procedure

The prime objective is to keep the maximum observed cooling of the underground $\max(\Delta\vec{T}_{i,j})$, caused by heat extraction through BHEs, as small as possible for the entire time span t. If extreme local cooling is avoided, the temperature distribution in the subsurface becomes smoother. This ideally results in a better efficiency of the heat pump, which is heavily influenced by the heat carrier fluid temperature of the BHE field, and consequently is controlled by the subsurface temperature. Another goal is the mitigation of the environmental impact of the system, which can play a role in case of environmental constraints for the design of BHE fields. Thus the

objective function of the proposed load assignment optimization reads

$$\text{minimize}(\max(\Delta\vec{T}_{i,j})) \tag{7}$$

With reference to the definition of $\Delta\vec{T}_{i,j}(t,\vec{q})$ given in Eq. (6), the objective function can also be expressed as:

$$\arg\min\left(\max(\Delta\vec{T}_{i,j}(t,\vec{q}))\right) \quad \forall(i,j,t)\in S \tag{8}$$

where $\vec{q}$ is the decision variable and S is a set of all spatial and temporal reference points defined by coordinates (i,j,t).

In some cases the maximum overall temperature change in the subsurface may not be influenced by the load assignment for certain time steps, depending on the field thermal parameters, the given load pattern and the inertia of the system. To capture these special cases, a secondary objective is introduced, which additionally minimizes the maximum temperature change within every single time step r of the defined load pattern:

$$\arg\min\left(\sum_{r=1}^{m}\max(\Delta\vec{T}_{i,j}(r,\vec{q}))\right) \quad \forall(i,j,t)\in S \quad t=r \tag{9}$$

To obtain a single objective function, which is sufficient for the given optimization problem, both Eqs. (8) and (9) are combined to

$$\arg\min\left(w\cdot\max(\Delta\vec{T}_{i,j}(t,\vec{q}))+\sum_{r=1}^{m}\max(\Delta\vec{T}_{i,j}(r,\vec{q}))\right) \quad \forall(i,j,t)\in S \tag{10}$$

where the second objective is only subsidiary and thus the primary objective is assigned a higher weight w than the secondary objective. In this study, w is set to 100.

To fulfill the energy demand required from the BHE field and to bar the optimizer from converging to the trivial solution, which is simply a complete switch-off of the BHE field, the adherence to the given energy demand is defined as a constraint. The sum of the loads $q_{k,r}$ for each time step r has to equal to the required energy E_r for the given time step:

$$E_r=\sum_{k=1}^{p}q_{k,r} \quad r=1,\ldots,m \tag{11}$$

A more detailed explanation of the structure of the resulting equation system can be found in [13].

3. Application case

3.1. Parameter settings and analytical model set-up

In our case-study, 25 BHEs are arranged in a square lattice that is analytically simulated by the superposition of Eq. (5) (Fig. 1). The distance between the BHEs is 10 m ($\Delta x = \Delta y = 10$ m) and the installation depth is 100 m. The subsurface is approximated as homogeneous isotropic media, with given properties as listed in Table 1, and a constant groundwater flow velocity is assumed in the x-direction (W–E). The annual energy load pattern, which has to be fulfilled, is given in Fig. 2. It was elaborated assuming a heat transfer rate of 50 W m^{-1}, with an annual runtime of 1800 h, which results in a total energy extraction of 225 MW h per year. The total energy extraction is subdivided into 12 monthly energy demands that reflect a seasonal operation mode in Central Europe, with exaggerated BHE use during the winter. The load pattern is repeated throughout the 10 years of simulation. The optimization procedure distributes the monthly loads among the individual BHEs while minimizing the relative temperature changes in the ground as estimated by the analytical solution.

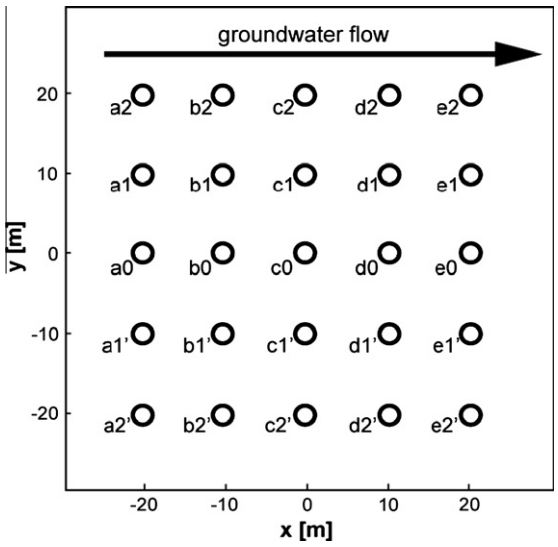

Fig. 1. Geometric arrangement and indices of simulated and optimized 25 BHEs.

Table 1
Parameter specifications for application case.

Parameter	Value
Porosity (n)	0.30
Density of solid (ρ_s)	2.65×10^3 kg m^{-3}
Density of water (ρ_w)	1.00×10^3 kg m^{-3}
Volumetric heat capacity of solid (C_s)[a]	1.92×10^6 J m^{-3} K^{-1}
Volumetric heat capacity of water (C_w)	4.19×10^6 J m^{-3} K^{-1}
Thermal conductivity of solid (λ_s)[a]	3.2 W m^{-1} K^{-1}
Thermal conductivity of water (λ_w)	0.6 W m^{-1} K^{-1}
Thermal conductivity of porous media (λ_m)	2.4 W m^{-1} K^{-1}
Longitudinal dispersivity (α_l)	1.0 m
Transverse dispersivity (α_t)	0.1 m
Length of the borehole (L)	100 m
Only used for the numerical model	
Undisturbed temperature (T_u)	12 °C
Borehole diameter (d)	0.15 m
Volumetric flow rate[b] (Q)	4×10^{-4} m^3 s^{-1}
Dynamic fluid viscosity[c] (μ)	1.14×10^{-3} kg m^{-1} s^{-1}
Density of circulating fluid[b] (ρ_w)	1×10^3 kg m^{-3}
Borehole thermal resistance (R_b)	0.07 K W^{-1} m^{-1}
Borehole internal thermal resistance (R_a)	0.25 K W^{-1} m^{-1}

[a] [26].
[b] Circulating fluid is water [40].
[c] At 15 °C.

As the role of advective heat transport due to groundwater flow is in the focus of this study, the influence of different groundwater flow velocities on optimized solutions is further scrutinized. A set of 15 scenarios is defined, which are considered representative of conditions found in sedimentary aquifers with moderate groundwater flow velocities (Table 2). The rationale is to create a variety of scenarios from conduction to advection dominated conditions, which can already be found within one order of magnitude velocity difference. In natural aquifers, velocities can vary over several orders of magnitude (e.g. [27]). Very small velocities of significantly less than 1 cm per day (sc. 1: 5.8×10^{-3} m d^{-1}, 6.7×10^{-8} m s^{-1}) are not inspected, since these are strongly conduction-dominated systems that may be approximated by assuming conduction only. The highest groundwater flow velocity is depicted by sc. 15, and it reaches 0.08 m d^{-1} (8.7×10^{-7} m s^{-1}). This is still not an extraordinary value having in mind that flow velocities of several meters per day are still realistic for some hydrogeological regimes. However, already noticeable advection-dominated conditions are

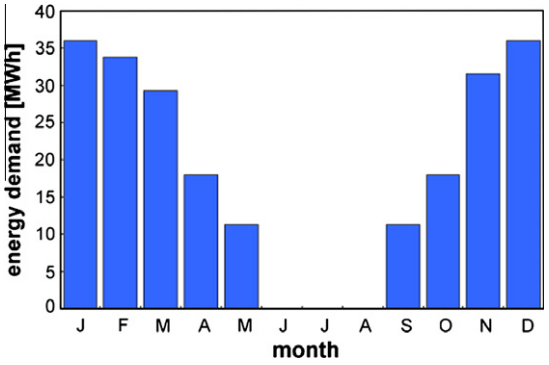

Fig. 2. Monthly energy demand of the BHE field assuming a specific energy extraction of 50 W m^{-1} and 1800 operating hours per year.

Table 2
Scenario-specific groundwater seepage velocities, v_a, corresponding hydraulic conductivity values, K, and Péclet numbers, Pe.

Scenario	K (m s^{-1})	v_a (m s^{-1})	Pe (–)
1	2.60×10^{-6}	8.7×10^{-8}	0.4
2	3.00×10^{-6}	1.0×10^{-7}	0.5
3	4.00×10^{-6}	1.3×10^{-7}	0.7
4	5.00×10^{-6}	1.7×10^{-7}	0.9
5	6.00×10^{-6}	2.0×10^{-7}	1.1
6	7.00×10^{-6}	2.3×10^{-7}	1.2
7	7.50×10^{-6}	2.5×10^{-7}	1.3
8	8.00×10^{-6}	2.7×10^{-7}	1.4
9	9.00×10^{-6}	3.0×10^{-7}	1.6
10	1.00×10^{-5}	3.3×10^{-7}	1.8
11	1.15×10^{-5}	3.8×10^{-7}	2.0
12	1.30×10^{-5}	4.3×10^{-7}	2.3
13	1.60×10^{-5}	5.3×10^{-7}	2.8
14	2.00×10^{-5}	6.7×10^{-7}	3.5
15	2.60×10^{-5}	8.7×10^{-7}	4.5

evident in sc. 15, and temperature signals propagate downgradient by several meters per season within the BHE field. The objective of the developed optimization procedure is strategic control of the dislocated BHE-specific thermal plumes.

Geological and, in particular, hydrogeological parameters are often not accurately known. Our scenario-based approach with different groundwater flow velocities will reveal the role of this parameter, which is governed by the effective hydraulic conductivity and the hydraulic gradient. The latter may vary during the year in a seasonal flow regime, and under such conditions an implicit representation of variability or uncertainty of this parameter, e.g. by employing multiple equally possible realizations (e.g., [30,31]), is favorable. Still, hydrogeological field measurements will be necessary to investigate the flow conditions. However, during implementation of a BHE field, the drilled boreholes offer a high resolution picture of the hydraulic gradient in the field. Thermal response tests, which are commonly conducted for planning BHE fields, can additionally be utilized to deduce the intensity of advection in the aquifer (e.g., [32]).

The depth-averaging model approach, as common in many line source applications for BHE simulation neglects potential ground heterogeneities and aquifer layering. When non-negligible, depth resolving numerical models may be preferred to the analytical ones used in our study. Independent of the model concept, however, in most cases still the superposition step and the optimization procedure can be applied given that the geometric BHE arrangement is pre-defined (e.g. [33]).

The Péclet number, Pe, for heat transport [34], as listed in Table 2, is a measure for the intensity of advection. It is calculated by:

$$Pe = \frac{v_a n L' \rho_w c_w}{\lambda_m} \tag{12}$$

with L' as the characteristic length, which, in this work, is set to the grid distance between the BHEs (10 m). Based on this definition, the Péclet number indicates the ratio between the heat transported by the moving groundwater and the heat solely transported by conduction.

3.2. Numerical simulation

Even if line-source-based simulation of BHE is standard, it is based on several simplifying assumptions. Among these are ideal, homogeneous conditions in the ground, which never exist. A relevant assumption for BHE field simulation is that the energy loads assigned to each BHE is known. In reality, however, energy extraction is achieved by circulating a cold heat carrier fluid, and the established temperature gradient forces conductive heat transfer from the ground. This means that the ground temperature in a BHE field is, to some extent, automatically balanced, and substantial local temperature anomalies thus are mitigated by smaller heat extraction from cold regions. In contrast, our approach is based on computationally efficient simulation and the optimization of loads. This presumes that working loads can be adjusted directly, e.g. by controlling the temperature of the heat carrier fluid. Showing that this control is reasonable depends on the benefit in comparison to standard practice, which means that all BHE in a field are operated similarly. To examine this in more detail, numerical simulations are carried out that compare the load-optimized strategies to non-optimized BHE operation.

Transient heat transport simulations for the fifteen scenarios are performed using the finite element code FEFLOW (version 6) [35]. A three-dimensional model with 100 layers of 1 m thickness (200 m × 200 m × 100 m), representing a homogeneous confined aquifer with steady flow, is set up. Twenty-five BHEs, each with a length of 100 m, are implemented. An initial uniform undisturbed temperature of 12 °C is assigned to the model, and further settings are given in Table 1. We chose the implemented analytical method of Claesson and Eskilson [36] for simulating the local heat transport processes within single U-type BHEs. The BHEs are operated using the single-load model [37,38]. Monthly loads are entered by scheduling operative hours of each borehole per month. For the non-optimized case, the operative hours per BHE are uniformly assigned. In contrast, for the optimized scenarios, we iteratively adjusted the operative hours for each BHE to achieve the determined optimal loads. All scenarios are simulated for 10 years and temperatures of the entire field are recorded at the end of each month. Additionally, the detailed numerical model allows for the monitoring of temperatures at the inlet and outlet of each BHE.

3.3. Simulation time and steady state condition considerations

The advective heat flow, in addition to conduction, further compensates the deficit from permanent energy extraction. The higher the groundwater flow velocity is, the less pronounced the temperature changes close to BHEs are. As a result, the time to reach steady state is shorter at high velocity [7,19]. This is also relevant for the 15 scenarios inspected in our study. Due to the different groundwater flow velocities, some scenarios reach steady-state condition at early times, while others show a transient temperature change until the end of the examined total operation time of 10 years. This is visualized in Fig. 3, where the evolution of mean temperature changes for all scenarios is compared.

The mean temperature change is estimated by:

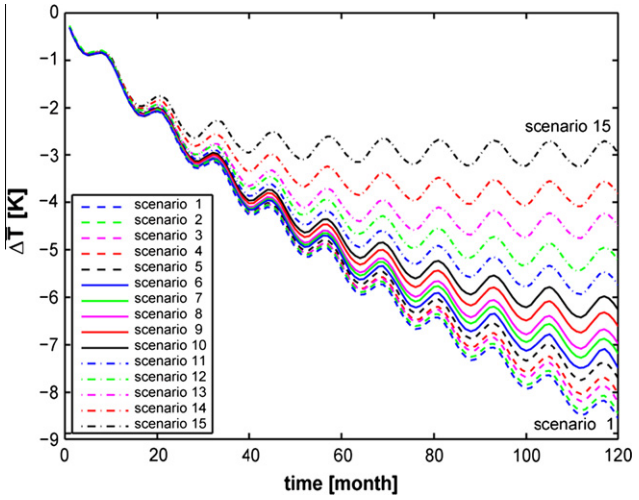

Fig. 3. Time-dependent mean temperature changes $\Delta\overline{T}$ within non-optimized BHE field (area of 40 m × 40 m) at a depth of 50 m. Dashed lines correspond to sc. 1–5, solid lines to sc. 6–10 and dash-dotted lines to sc. 11–15.

$$\Delta\overline{T} = (m \times n)^{-1}\left(\sum_{i=1}^{m}\sum_{j=1}^{n}\Delta T_{ij}\right) \tag{13}$$

where ΔT_{ij} is the temperature change at each location (i, j) within the area $m \times n$ where the BHEs are located. All the undulating time series in Fig. 3 reflect the seasonal energy extraction, but those scenarios with high velocity are less affected. Temperature decrease is less pronounced and, in particular for sc. 12–15, the trends stabilize, which indicates that a steady state is (nearly) reached. We compared the maximum difference of $\Delta\overline{T}$ at the end of the last two successive years. For these scenarios, this difference is smaller than 1% after 72 (sc. 15), 84 (sc. 14), and 96 (sc. 13) months. With a criterion of 2%, scenario 12 takes 108 months to reach a steady state. In summary, high flow velocities ($Pe > 2.3$) allow for a (quasi) steady-state condition before the end of the considered period of 10 years is reached, whereas conduction in scenarios 1 to 11 ($Pe < 2.3$) is significant enough so that transient conditions prevail.

4. Results and interpretation

4.1. Temperature fields and profiles

From the 15 scenarios, four are sampled that span the range of inspected groundwater flow velocities: the two extremes with the lowest (sc. 1, $Pe = 0.4$) and highest velocity (sc. 15, $Pe = 4.5$), as well as intermediate cases sc. 5 ($Pe = 1.1$) and sc. 10 ($Pe = 1.8$). Fig. 4 depicts the central ($z = 50$ m depth) temperature distribution from numerical simulation for the optimized and non-optimized cases. A total operation time of 10 years is simulated, and the plotted temperatures reflect the conditions in December, that is, in the middle of the heating season. All BHE fields supply the given seasonal energy demand (Fig. 2), and accordingly, extract the same amount of energy each month.

As expected, the temperature anomaly that is induced from operating the BHE field is influenced by groundwater flow. At very small velocity, the most pronounced ground cooling is observed within the field, and it nearly symmetrically diminishes outside the field. The temperature plume moves downgradient at increasing velocity, is displaced from the center of the BHE field, and appears significantly elongated for the most advection dominated sc. 15.

For each scenario, the plumes have a comparable shape independent of the operation mode. However, strongest cooling is observed for the non-optimized cases. The optimization regulates individual BHE operation in order to avoid local cooling in favor of smoother temperature changes. This is most beneficial for conduction-dominated conditions. For instance, in sc. 1, the temperature maximally decreases by 10.4 K without and by only 7.3 K with optimization, which means a difference of more than 3 K. This difference in max ΔT, as well as overall cooling, becomes smaller the more groundwater flow balances the mounting energy deficits by advection. For the conditions with highest velocity, sc. 15, max ΔT reaches 5.7 K without and 3.7 K with optimization. In this non-optimized scenario, the center of the cold plume is found around the last downgradient column ('e', Fig. 1) of the BHE array. This center is smoothed when the BHEs are individually regulated, and also shifted further downgradient, that is, if possible outside of the BHE field.

A closer insight is provided by Fig. 5, which inspects the differences in max ΔT for the selected four scenarios in the x-direction of groundwater flow and perpendicular to it, both along the centerline of the BHE array. Negative values indicate that the temperature at a given location of the non-optimized scenarios is lower than for the optimized ones and vice versa.

As expected, the temperature differences perpendicular to the regionally uniform groundwater flow are symmetric (Fig. 5a). Since optimization especially mitigates the energy extraction by the BHEs in the center of the field, differences are most significant at BHEs 'c0' and 'c1'. The higher the groundwater flow velocity, the more advective heat is supplied and thus the smaller the differences between optimized and non-optimized scenarios. For sc. 15, advection is exploited more by the optimized lateral BHEs, 'c2', which is reflected by the slightly stronger cooling at these positions of the temperature difference curves.

Along the horizontal centerline (Fig. 5b), each trend is specific for the simulated conditions with highest differences at the locations of the BHEs. The simulated cooling with optimal loads of sc. 1, 10 and 15 is always minor. Sc. 5 is special – it shows a stronger cooling (difference > 1 K) at the location of the first BHE ('a0', Fig. 1). Apparently, this is compensated by the higher temperatures at the other downgradient BHE locations (difference of nearly −4 K). The energy extraction rate of BHE 'a0' for this month is 32.66 W m^{-1}, while for the downgradient BHEs 'b0'–'e0' have optimized rates of 25.18 W m^{-1}, 15.68 W m^{-1}, 11.33 W m^{-1} and 11.45 W m^{-1}. The energy extraction rates for the same BHEs in the non-optimized case are 22.88 W m^{-1}, 22.88 W m^{-1}, 22.96 W m^{-1}, 22.88 W m^{-1} and 22.96 W m^{-1} ('a0'–'e0'). Obviously, the concerted BHE array takes advantage of the energy carried by the groundwater more efficiently. This exemplarly shows that for a given month in the optimal load pattern, each BHE is adjusted depending on position, groundwater flow velocity and the current time step.

An important feature of Fig. 5, particularly in the direction of groundwater flow (Fig. 5b), is the occurrence of four different curve shapes. These four are also characteristic for the other scenarios. Similar curves are observed for sc. 1–2 ($Pe \leqslant 0.5$), sc. 3–6 ($Pe = 0.7–1.2$), sc. 7–12 ($Pe = 1.3–2.3$), and sc. 13–15 ($Pe \geqslant 2.8$). They, apparently, reflect that a small number of optimized load patterns exists, which is selected and adjusted depending on the groundwater flow velocity and supplied energy demand.

4.2. Optimized load patterns

In Fig. 6, the spatial temperature distributions during the last entire heating season (9th year) of the selected optimized scenarios are shown. The relative contribution (i.e. monthly normalized load) of each BHE is visualized by the gray scale of the circle marker. The figures show the initial stage of the heating season

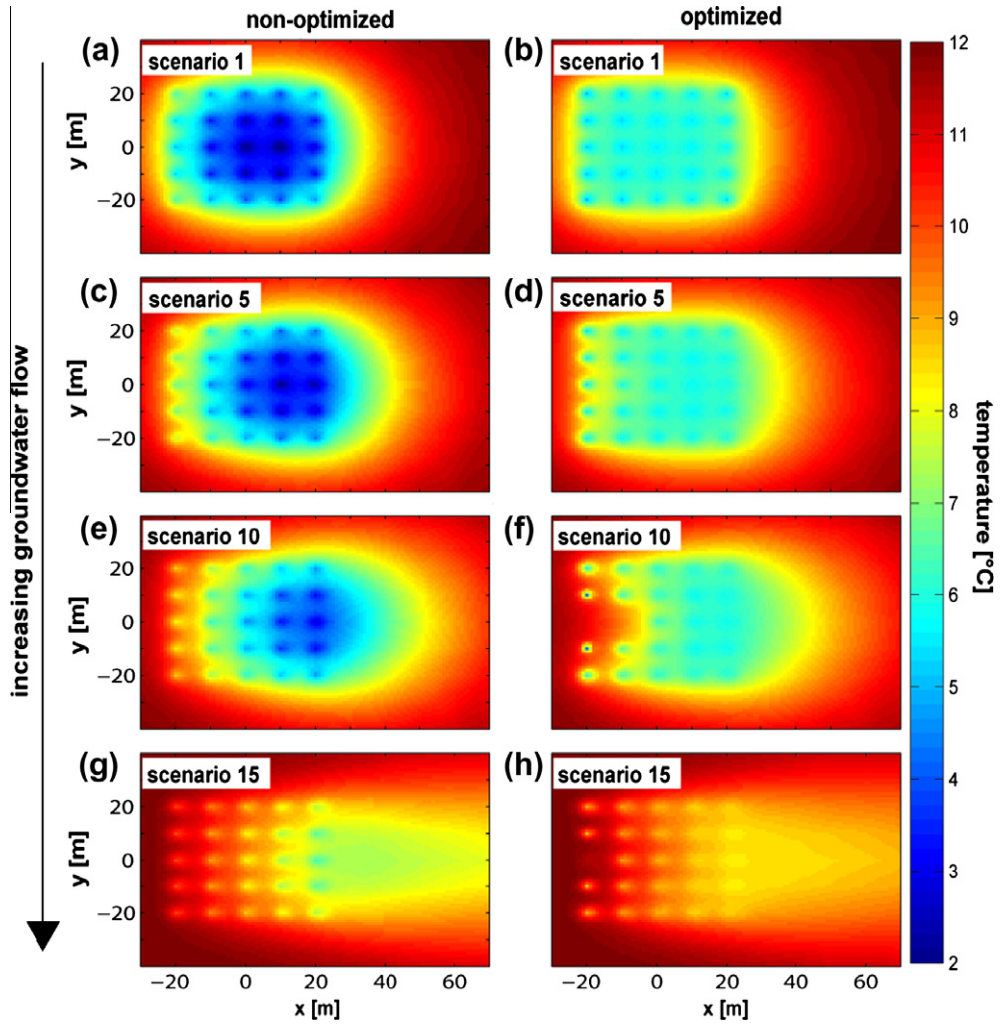

Fig. 4. Spatial temperature distribution for the non-optimized (subplots a, c, e and g) and optimized cases (subplots b, d, f and h) for selected scenarios (sc. 1, 5, 10 and 15) after 10 years (31st December). The depicted fields correspond to the temperature distribution at the 50th layer ($z = 50$ m).

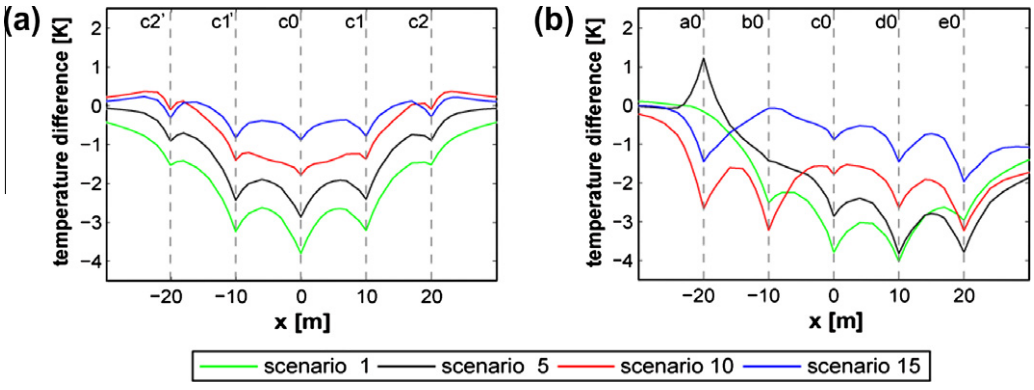

Fig. 5. Temperature difference between non-optimized and optimized cases for selected scenarios: (a) central column ('c', Fig. 1) perpendicular to flow and (b) central row (a0–e0, Fig. 1) in direction of groundwater flow.

(in September), the month with highest demand (in January) and the last month of the heating season (in May).

At the beginning of the heating season, for the scenarios with higher groundwater flow velocity (sc. 10 and 15), the BHEs located downgradient (columns c–e; Fig. 1) are activated first. In order to maximize energy extraction from outside the BHE field, the BHEs at the fringe provide most of the energy demand. The upgradient BHEs, as well as the central BHEs in the columns 'c' and 'd', are shut off. An attractive strategy, evidently, is keeping the temperature highest in the center and preparing the system for the higher energy demand scheduled for the next months. The energy demand reaches its maximum in January, all BHEs in sc. 15 are on and almost all (23 of 25 BHEs) are activated in sc. 10. At this stage, the upgradient BHEs in column 'a' have the highest energy extraction

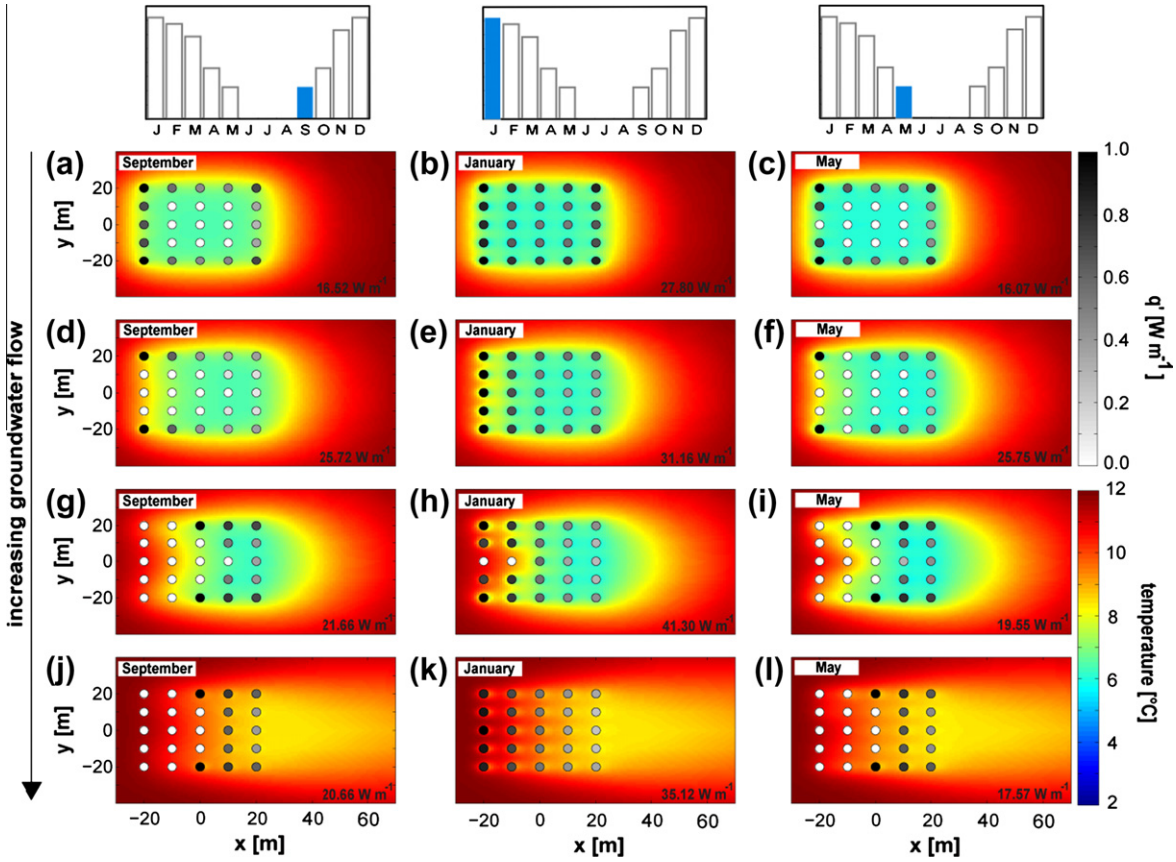

Fig. 6. Temperature distribution and BHE extraction rates for the optimized selected scenarios (scenarios 1, 5, 10 and 15, from top to bottom) for 3 months of the entire last heating period (9th year). Each circle represents a BHE, with its corresponding normalized load in grayscale (maximal load is shown in each plot). Darker color shades denote higher BHE loads. The subsurface temperature distribution at a depth of 50 m is illustrated with colors. (For interpretation of the references to color in this figure legend, the reader is referred to the web version of this article.)

rates. This way, the system takes advantage of the surplus energy brought by the moving groundwater. The extraction rates successively decrease downgradient. Then, at the end of the heating season in May, the load pattern of the BHEs is similar to that in September.

For the scenarios with lower groundwater flow velocity (sc. 1 and 5), the operation strategy is different. At the beginning of the heating season, again the BHEs in the center are off. However, now, all BHEs at the lateral rows are activated. In sc. 1, the highest loads are assigned to the BHEs in the upgradient corners (position 'a2') and they continuously shrink downgradient. In sc. 1 groundwater flow is minimal, and the optimal load pattern accentuates all corner BHEs ('a2', 'e2'). This scheme is also kept for the peak of the heating season in January. Both scenarios show a similar use of the BHEs, with more upgradient energy extraction. In the more conductive scenario (sc. 1), the highest energy extraction rates are still in the corners and decrease towards the center. Again, at the end of the heating season, a similar operation of the BHEs is observed as in the beginning.

In general, two operation patterns for the 25 examined BHE fields are identified. For high groundwater flow velocities, the operation of the BHE follows a column-wise strategy. In all scenarios 12–15, the optimal tactic for seasonal energy extraction is to start with the downgradient BHEs, and then activate increasingly the upgradient ones, while reducing the loads downgradient. The downgradient movement of the cooled zones is strategically integrated in the optimized load pattern. The optimal usage of a column thus depends on the energy demand of each consecutive month.

For lower groundwater velocities, conduction comes more into the fore and hence, a more radial pattern is observed. BHEs at the corners are turned on first and run permanently, with a higher emphasis on the downgradient ones depending on the role of advection. Under low-advection conditions, these BHEs have least interaction with neighboring BHEs. In contrast, central BHEs mean strongest competition for conductive heat supply. Accordingly, the interior BHEs are activated or deactivated in a radial way. For the inspected total simulation time of 10 years, this radial pattern is most apparent for the high conduction end members, sc. 1–3. In particular, for sc. 4–11, a mixed pattern with column-wise and radial scheme is found.

4.3. Mean temperature in BHE field and heat carrier fluid

In order to compare optimized to standard operation mode, Eq. (13) is applied for the 3 months of the final heating season. Depending on the scenario-specific *Pe*, the induced mean temperature changes $\Delta\overline{T}$ for January is shown in Fig. 7a. In addition, the difference of $\Delta\overline{T}$ between optimized and non-optimized conditions for September, January and May is depicted. This difference appears to be always positive, it reaches between 0.37 K and 1.96 K, and it is nearly the same for the different months. This means that BHE field optimization does not only mitigate local cooling but also the average temperatures in the field are less altered. Since groundwater flow compensates, to some extent, the deficits from energy extraction, the difference shrinks in the more advection-dominated scenarios. A nearly linear trend is observed, whereas

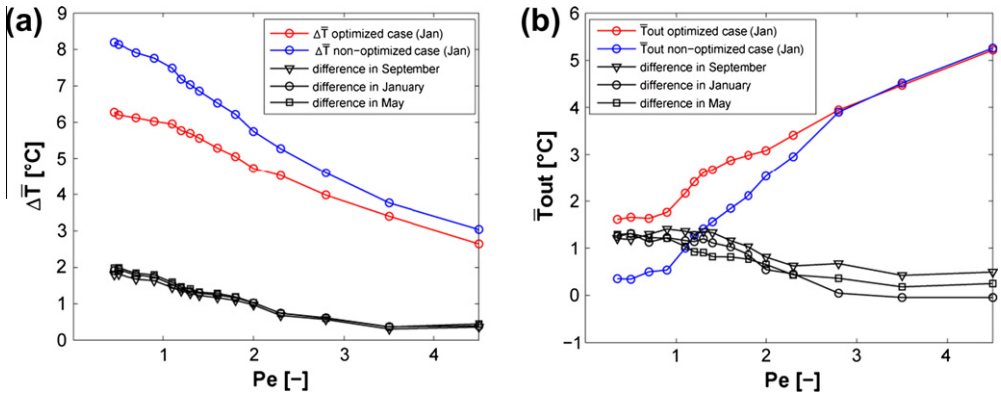

Fig. 7. (a) Mean temperature change $\Delta\overline{T}$ in the BHE field at a depth of 50 m for all scenarios (optimized and non-optimized); (b) monthly mean temperature $\overline{T}_{out}$ of the BHE working fluid. Temperature changes (a) and absolute values (b) are plotted as functions of the Péclet number, which increases with the contribution of advective heat transport. The results are shown only for January (red and blue lines with circles for optimized and non-optimized, respectively), the black curves show the difference between optimized and non-optimized cases in September, January and May. (For interpretation of the references to color in this figure legend, the reader is referred to the web version of this article.)

for the most extreme cases, sc. 14, 15 ($Pe \geqslant 3.5$), this difference becomes very small and stabilizes.

The efficiency of a heat pump in GSHP systems strongly depends on the temperature of the heat carrier fluid circulating through the BHE (e.g., [24]). If aboveground thermal losses are negligible, this temperature equals the temperature at the outlet of a BHE (T_{out}). Fig. 7b compares the mean (mixed) temperatures for all BHEs $\overline{T}_{out}$ for the optimized and non-optimized cases in January of the 10th year. Also, similar to Fig. 7a, the differences between both cases in January, as well as in September and May, are shown. These temperatures are obtained by averaging the monthly BHE outflow temperature predicted by the numerical model. Slight numerical inaccuracies are reflected in the non-uniform curves in Fig. 7b. The finite element mesh for this study was developed following the direct estimation of the nodal distance for BHE nodes [39]. However, in order to keep the computational burden at a minimum, the mesh was discretized in two different sections, one very dense around the BHE field and a coarser mesh outside of the BHE field. The slightly non-symmetrical distribution of the elements probably causes small variations in the borehole wall temperatures, which are used to calculate $\overline{T}_{out}$.

Optimized configurations result, although not explicitly included in the optimization problem formulation, generally in higher output temperatures $\overline{T}_{out}$ of the heat carrier fluid. The January values show that the difference between optimized and non-optimized depend on the groundwater flow velocity. Roughly, three characteristic ranges for Pe can be distinguished: For $Pe < 1$ (sc. 1–4), conduction dominates, the output temperatures are independent of the flow velocity, and benefit from optimization is maximal. Here, the heat carrier fluid is more than 1 K higher. Between $Pe = 1.1$ (sc. 5) and 2.3 (sc. 12), as observed for the average ground temperatures in Fig. 7a, the impact from advection comes more into the fore, and cooling of the ground is mitigated. Since, for the study case, the seasonal energy demand is kept constant, differences between optimized and non-optimized operation mode decline. For very high velocities, sc. 13–15 ($Pe \geqslant 2.8$), we observe no difference or the difference remains constant on a small value as shown for September and May. However, note that the averaging method used for estimating $\overline{T}_{out}$ disregards local variations at individual BHEs, which may be of relevance in practice when more than one heat pump is operated.

5. Discussion and conclusions

Low enthalpy geothermal technologies are established and, once installed, supply space heat and domestic hot water for decades. Fields of multiple adjacent BHEs, which in the long run, cool the ground over great volumes, often accomplish high-energy demand. Often, aquifers exist, which are affected by the cooling, while advective heat transport from flowing groundwater additionally balances the deficits. Integrating the advection into the planning of BHE fields is not common, and it is only done indirectly by introducing an effective thermal conductivity that is higher than the actual one (e.g. [32]). The study here demonstrates that for a given BHE field, case-specific individual BHE operation mode offers benefits to standard applications, where BHEs are all operated the same. As an objective, we chose to avoid extreme local cooling of the ground while guaranteeing a given seasonally variable energy demand. An efficient linear-programming based solution procedure that combines superimposed moving line source equations is developed, and the performance of optimized solutions is inspected by post-optimization high-resolution numerical models.

The major findings are that ideal adjustment of BHE-specific, monthly energy extraction rates (loads) produces typical load patterns that depend on time and groundwater flow velocity. The patterns change from the beginning of the heating season to the peak demand month, and those at the end are similar to those at the beginning of the season. Formulating the optimization problem for the entire operation period (in our study case 10 years) enables pro-active management where, for example, the BHE active in the early season prepares efficient operation in the peak time. Also, long-term transient conditions, which exist in the low groundwater flow velocity scenarios of our study, provoke a slight change in the patterns from year to year. If groundwater flow is small (here $Pe < 1$), radial patterns are suggested, where most energy is extracted by the BHEs at the borders. Increase of flow velocity generates optimized patterns that, advantageously, are oriented at the flow direction. For example, in the lattice BHE field in the study case, a column-wise pattern is found, where the season starts and ends, with downgradient BHE operation.

We inspected the role of increasing advection for a fixed energy demand, and as a result, benefits from optimization decrease with flow velocity. In practice, however, higher velocity may be accounted for by a higher effective thermal conductivity, and thus the specific energy extraction in standard applications is augmented. Therefore, due to the assumptions particular to the study case in this work, potential benefits from optimized BHE operation patterns have to be clarified based on the individual conditions. Even so, it is shown that improvements could always be achieved by automatic optimization, with more balanced ground cooling and mostly higher temperatures in the heat carrier fluid. These

may be further improved also by considering the positioning of the BHE in the optimization framework, and if energy injection for cooling of buildings during the summer is included.

Acknowledgements

This work was supported by the Federal Ministry for Education and Research (BMBF) scholarship program for International Postgraduate Studies in Water Technologies (IPSWaT), the German Federal Environmental Foundation (DBU), and the EU FP7 ECO-GHP Project. The authors would like to thank the technical support team from WASY and Christian Gabriel for the help with the FEFLOW modules and data post-processing. Finally, we thank the four anonymous reviewers for their helpful comments and suggestions that improved the quality of the manuscript.

References

[1] Ozgener L, Hepbasli A, Dincer I. A key review on performance improvement aspects of geothermal district heating systems and applications. Renew Sustain Energy Rev 2007;11:1675–97.
[2] Lund JW, Freeston DH, Boyd TL. Direct utilization of geothermal energy 2010 worldwide review. In: Proceeding of the 2010 world geothermal congress; 2010.
[3] Bayer P, Saner D, Bolay S, Rybach L, Blum P. Greenhouse gas emission savings of ground source heat pump systems in Europe: a review. Renew Sustain Energy Rev; in press. http://dx.doi.org/10.1016/j.rser.2011.09.027.
[4] Fujii H, Itoi R, Fujii J, Uchida Y. Optimizing the design of large-scale ground-coupled heat pump systems using groundwater and heat transport modeling. Geothermics 2005;34:347–64.
[5] Gao Q, Li M, Yu M, Spitler JD, Yan YY. Review of development from GSHP to UTES in China and other countries. Renew Sustain Energy Rev 2009;13:1383–94.
[6] Ozgener O, Hepbasli A, Ozgener L. A parametric study on the exergoeconomic assessment of a vertical ground-coupled (geothermal) heat pump system. Build Environ 2007;42:1503–9.
[7] Diao N, Li Q, Fang Z. Heat transfer in ground heat exchangers with groundwater advection. Int J Therm Sci 2004;43:1203–11.
[8] Katsura T, Nagano K, Narita S, Takeda S, Nakamura Y, Okamoto A. Calculation algorithm of the temperatures for pipe arrangement of multiple ground heat exchangers. Appl Therm Eng 2009;29:906–19.
[9] Rybach L, Eugster WJ. Sustainability aspects of geothermal heat pump operation, with experience from Switzerland. Geothermics 2010;39:365–9.
[10] Hellstrom G, Sanner B. EED – earth energy designer, version 1.0, user's manual. Wetzlar: Prof. Dr. Knoblich & Partner GmbH; 1997.
[11] Spitler JD. GLHEPRO: a design tool for commercial building ground loop heat exchangers. In: Fourth international heat pumps in cold climates conference; 2000.
[12] Hellström G, Mazzarella L, Pahud D. Duct ground storage model – TRNSYS version. Lund: Department of Mathematical Physics, University of Lund; 1996.
[13] de Paly M, Hecht-Méndez J, Beck M, Blum P, Zell A, Bayer P. Optimization of energy extraction for closed shallow geothermal systems using linear programming. Geothermics 2012;43:57–65.
[14] Eskilson P. Thermal analysis of heat extraction boreholes. Lund: Department of Mathematical Physics, University of Lund; 1987.
[15] Sutton MG, Nutter DW, Couvillion RJ. A ground resistance for vertical bore heat exchangers with groundwater flow. J Energy Res Technol 2003;125:183–9.
[16] Molina-Giraldo N, Bayer P, Blum P. Evaluating the influence of thermal dispersion on temperature plumes from geothermal systems using analytical solutions. Int J Therm Sci 2011;50:1223–31.
[17] Molina-Giraldo N, Blum P, Zhu K, Bayer P, Fang Z. A moving finite line source model to simulate borehole heat exchangers with groundwater advection. Int J Therm Sci 2011;50:2506–13.
[18] Carslaw HS, Jaeger JC. Conduction of heat in solids. New York: Oxford University Press; 1959.
[19] Chiasson AC, Rees SJ, Spliter JD. A preliminary assessment of the effects of ground-water flow on closed-loop ground-source heat pump systems. ASHRAE Trans 2000;106:380–93.
[20] Haehnlein S, Molina-Giraldo N, Blum P, Bayer P, Grathwohl P. Cold plumes in groundwater for ground source heat pump systems. Grundwasser 2010;15:123–33 [in German].
[21] Fan R, Jiang YQ, Yao Y, Shiming D, Ma ZL. A study on the performance of a geothermal heat exchanger under coupled heat conduction and groundwater advection. Energy 2007;32:2199–209.
[22] Lee CK, Lam HN. Effects of groundwater flow direction on performance of ground heat exchanger borefield in geothermal heat pump system using 3-D finite difference method. In: 10th IBPSA building simulation conference; 2007.
[23] Wang H, Qi C, Du H, Gu J. Thermal performance of borehole heat exchanger under groundwater flow: a case study from Baoding. Energy Build 2009;41:1368–73.
[24] Bernier M. Closed-loop ground-coupled heat pump systems. ASHRAE J 2006;48:12–9.
[25] Haehnlein S, Bayer P, Blum P. International legal status of the use of shallow geothermal energy. Renew Sustain Energy Rev 2010;14:2611–25.
[26] Butscher C, Huggenberger P, Auckenthaler A, Baenninger D. Risk-oriented approval of borehole heat exchangers. Grundwasser 2011;16:13–24 [in German].
[27] de Marsily G. Quantitative hydrogeology. Orlando: Academic Press; 1986.
[28] Metzger T, Didierjean S, Maillet D. Optimal experimental estimation of thermal dispersion coefficients in porous media. Int J Heat Mass Transfer 2004;47:3341–53.
[29] Chiasson A, O'Connell A. New analytical solution for sizing vertical borehole ground heat exchangers in environments with significant groundwater flow: parameter estimation from thermal response test data. Hvac&R Res 2011;17:1000–11.
[30] Bayer P, Bürger CM, Finkel M. Computationally efficient stochastic optimization using multiple realizations. Adv Water Resour 2008;31:399–417.
[31] Bayer P, de Paly M, Bürger CM. Optimization of high-reliability-based hydrological design problems by robust automatic sampling of critical model realizations. Water Resour Res 2010;46:W05504.
[32] Wagner V, Bayer P, Kuebert M, Blum P. Numerical sensitivity study of thermal response tests. Renew Energy; in press. http://dx.doi.org/10.1016/j.renene.2011.11.001.
[33] Beck M, Hecht-Méndez J, de Paly M, Bayer P, Blum P, Zell A. Optimization of the energy extraction of a shallow geothermal system. In: IEEE congress on evolutionary computation (CEC); 2010.
[34] Domenico PA, Schwartz FW. Physical and chemical hydrogeology. 2nd ed. New York: John Wiley & Sons Inc.; 1990.
[35] Diersch HJG. FEFLOW 6-user's manual. Berlin: Wasy GmbH; 2010.
[36] Claesson J, Eskilson P. Conductive heat extraction to a deep borehole: thermal analyses and dimensioning rules. Energy 1988;13:509–27.
[37] Signorelli S, Kohl T, Rybach L. Sustainability of production from borehole heat exchanger fields. In: Proceeding of the 29th workshop on geothermal reservoir, engineering; 2004.
[38] Rybach L, Eugster WJ. Sustainability aspects of geothermal heat pumps. In: Proceedings 27th workshop on geothermal reservoir, engineering; 2002.
[39] Wasy, White papers vol. 5. DHI-Wasy GmbH, Berlin; 2010.
[40] Al-Khoury R, Kolbel T, Schramedei R. Efficient finite element modeling of shallow geothermal systems. Comput Geosci 2010;36:1301–15.